Journal of Microscopy, Vol. 202, Pt 1, April 2001, pp. 84–93.
Received 28 August 2000; accepted 1 December 2000

Optical near-field harmonic demodulation in apertureless microscopy

N. MAGHELLI*, M. LABARDI*, S. PATANÈ†, F. IRRERA† & M. ALLEGRINI*†
**INFM-Unità di Pisa Università, Via F. Buonarroti 2, I-57127 Pisa, Italy*
†INFM and Dipartimento di Fisica della Materia e Tecnologie Fisiche Avanzate, Università di Messina, Salita Sperone 31, I-98166 Messina, Italy

Key words. Apertureless, artefact, demodulation, harmonics, microscopy, near field, tuning fork.

Summary

Spatial derivatives of the optical fields scattered by a surface can be investigated by apertureless near-field optical microscopy by modulating sinusoidally the probe to sample distance and detecting the optical signal at the first and higher harmonics. Demodulation up to the fifth harmonic order has been accomplished on a sample of close-packed latex spheres by means of the silicon tip of a scanning interference apertureless microscope. The working principles of such microscope are reviewed. The experimental configuration used comprises a tuning-fork-based tapping-mode atomic force microscope for the distance stabilization, and a double-modulation technique for complete separation of the topography tracking from the optical detection. Simple modelling provides first indications for the interpretation of experimental data. The technique described here provides either artefact-free near-field optical imaging, or detailed information on the structure of the near fields scattered by a surface.

1. Introduction

Scanning near-field optical microscopy (SNOM) of apertureless (or scattering) type is based on the collection of light scattered by a nanometre-size particle (also named nanoantenna), comprising the probe, that is placed in close proximity to the illuminated sample surface. A SNOM image is reconstructed by raster scanning such probe on the surface while maintaining the relative distance within the near-field zone $z << \lambda$.

Resolution of apertureless microscopes, as opposed to aperture-type SNOMs, is not limited by the optical aperture size realistically achievable (about 20 nm). On the contrary, fabrication technology of atomic force microscopy (AFM) tips, commercially available and usable as light scatterers, offers curvature radii down to a few nanometres.

The scattering intensity fall due to reduction of tip size imposes challenging sensitivity limits to the apertureless microscopy experiments. Detection of amplitude of light fields (instead of their intensity) by interferometric techniques has pushed down such limits by orders of magnitude, allowing imaging of optical structures on the nanometre scale (Zenhausern *et al.*, 1994, 1995). Some debate on the contrast mechanisms of apertureless microscopy (Garcia & Nieto-Vesperinas, 1995) is accompanied by unexpectedly good results obtained with apertureless SNOM exploiting the intensity detection (Bachelot *et al.*, 1997; Hamann *et al.*, 1998), showing that full comprehension of this field is certainly not yet achieved.

A different issue in apertureless microscopy is represented by the large background level present in the optical measurements. An effective technique for background rejection is the vertical modulation of the probe and the synchronous detection of the optical signal. Modulation of the vertical probe position has customarily been applied in apertureless near-field microscopy since its conception (Zenhausern *et al.*, 1994), and methods allowing such modulation are also available with aperture SNOMs (Lieberman *et al.*, 1996; Brunner *et al.*, 2000).

The amount of light collected by the detector depends indeed on the probe to sample distance z. By oscillating the probe on the sample in the vertical (z) direction, the optical signal $W(z)$ is characterized by an average value and a modulated part. If the dependence of optical signal on distance was linear, the average value, comprising the background, would correspond to the value taken by the optical signal when the probe is at the midpoint of the oscillation in the case of no modulation. The optical signal modulation would be sinusoidal, and the modulation depth would be the measure of the z-gradient of $W(z)$. Such a signal, comprised by a first harmonic term only, would be

Correspondence: S. Patanè. Tel.: +39 090 6765 393; fax: +39 090 391 382; e-mail: salvatore.patane@unime.it

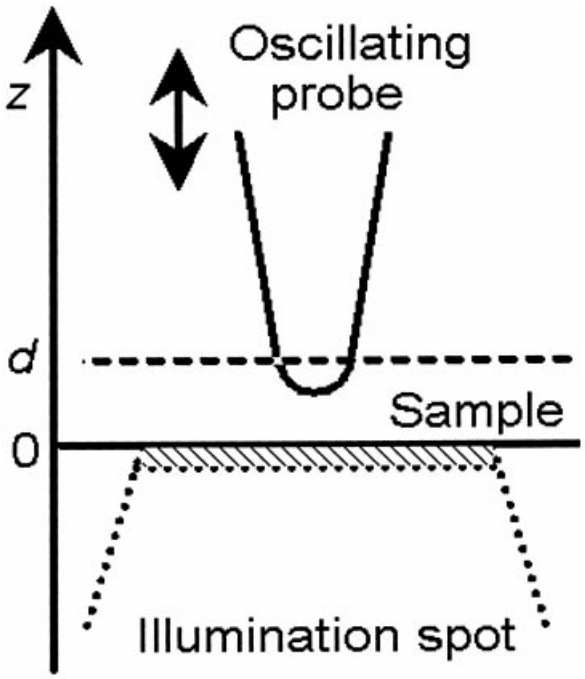

Fig. 1. Sketch of the tip–sample system of an apertureless near-field microscope.

measurable by the lock-in technique referenced to the *z*-position modulation frequency. If the dependence on distance was nonlinear, the average value would not correspond to the midpoint value anymore, and further, higher harmonics would appear in the optical signal modulated part. Even so, these harmonics may be measured by the *n*th harmonic lock-in technique. Thus, the main conclusions regarding vertical probe modulation in apertureless SNOM are that: (1) the average (d.c.) optical signal is modified by the presence of the modulation; (2) the modulated (a.c.) optical signal at the first and higher harmonics contains information on the dependence of the optical signal itself on distance.

Artefacts due to vertical probe motion are generally of relevant weight in SNOM compared to other kinds of scanning probe microscopies, owing to the fact that the investigated interactions involve also propagating waves. Let us refer to Fig. 1, where the probe and the sample holder of an apertureless SNOM are sketched, for the following analysis. The scan area is supposed to be illuminated by a focused laser beam. Thus, the whole system (sample, tip, remote parts) are concerned by light, and possibly some of it can end up on the detector (placed anywhere), after one or more reflections or after scattering from any of the parts of the system. The beam focusing is intended to reduce the region concerned by light as well as to concentrate it on the probe location.

Probe to sample distance adjustment is necessary in SNOM to fulfil the near-field condition $z << \lambda$. A *z*-motion artefact shows up when the adjustment itself is the origin of a change of the optical signal. Usually, the distance is controlled by exploiting a scanning probe technique, different from the optical one, like scanning tunnelling microscopy (STM) for conductive tip and sample, or more often by AFM. Such choice is imposed by the observation that, apart from very special cases, the optical signal is not characterized by a monothonical dependence on distance whatsoever. Therefore, the distance control provides a nanometre resolution topography tracking system that is independent of the optical features of the sample. Such tracking is performed by lifting or lowering the probe (or the sample) while the lateral raster scanning is performed in order to reconstruct an image. The vertical movement might be translated into an optical signal that is not related to the optical properties of the sample. Such an optical signal, called a *z*-motion artefact, is characterized by the same resolution of the auxiliary distance control detection system (STM or AFM), that is generally higher than the purely optical one. The *z*-motion artefact can be mixed with the true optical information that is derived from the different scattering of the probe when located on different parts of the sample, characterized by the optical resolution allowed more strictly by the probe shape and size, sample type and measurement configuration.

Figure 1 clearly shows that the choice of adjusting the *z*-position of the sample leads to strong variations of the background light, as the illuminating beam is focused on the sample. If probe *z*-adjustment is made instead, much less influence must be expected because the probe aspect ratio is rather high and its illuminated portion is much smaller with respect to the illumination spot. Thus, far lower artefact levels should be expected by moving the probe. Different considerations are valid for the lateral raster scanning motion that can be accomplished by the tip as well as by the sample with no introduction of *z*-motion artefacts.

First harmonic detection of the optical signal is often performed in apertureless microscopes adopting tapping-mode AFM for topography tracking (Zhong *et al.*, 1993). In tapping (also named intermittent contact) mode, the AFM tip is kept in vertical vibration at high amplitudes (10–200 nm peak-to-peak typically). Therefore, in such microscopes it is particularly convenient to detect the optical signal modulation due to the tip oscillation, provided that the used lock-in amplifier is referenced to the actual tip oscillation and not just to the excitation signal. A disadvantage of this kind of synchronous detection is that any perturbation to the topography tracking system will be immediately reflected on the optical image, leading to enhancement of topographical artefacts.

Optical signal demodulation performed at higher harmonics has been recently analysed both experimentally (Hillenbrand & Keilmann, 2000; Knoll & Keilmann, 2000; Labardi *et al.*, 2000a) and theoretically (Adam *et al.*, 2000).

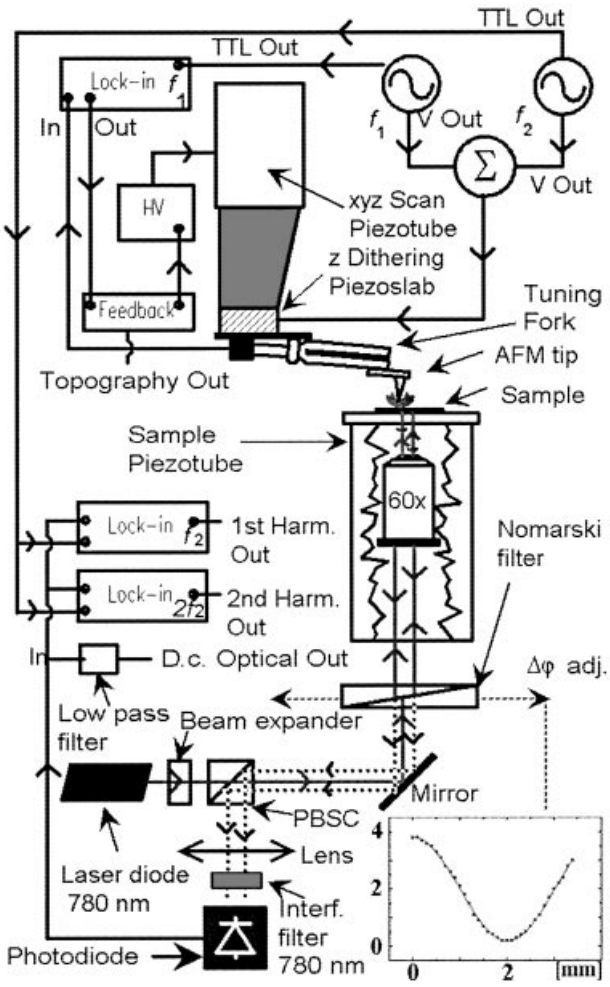

Fig. 2. Sketch of our higher-harmonics scanning interference apertureless microscope (described in the text). In the inlet is reported the measured interferometer fringe which shows a visibility of 90%.

This technique improves the resolution and shows capability of artefact suppression to a large extent. The general finding is that a lock-in measurement of the optical signal has the effect of a bandpass filter centred on the spatial frequencies associated with the used oscillation amplitude. Hence, near fields are effectively discriminated from far fields, as well as from *z*-motion artefacts (Hecht *et al.*, 1997), as in general their spatial dependence is also far-field-like.

Increasing the harmonic order n leads to overall signal reduction and to artefact suppression both of order $(d/L)^n$ where $d = 2\pi/f_{xy}$ is the distance associated with the spatial frequency f_{xy} of interest, and λ the wavelength. The contribution of near fields with respect to far field and artefacts is enhanced by increasing the harmonic order. Such behaviour is also referred to as effective tip sharpening due to the vertical modulation (Knoll & Keilmann, 2000).

A good compromise between signal magnitude and near-field enhancement has been shown experimentally to be the second harmonic, both with dielectric (Labardi *et al.*, 2000a) and metallic (Hillenbrand & Keilmann, 2000) tips; measurements up to the third harmonic have been reported with such tips (Knoll & Keilmann, 2000). However, in the present work we have observed contributions to the optical field up to fifth harmonic, with the silicon tips used in our scanning interference apertureless microscope (SIAM). This performance was possible owing to the good stability and signal-to-noise ratio (S/N) of our set-up, exploiting a double-modulation technique (Labardi *et al.*, 2000a) briefly described in Section 2 along with other technical features of the set-up. Simple modelling, derived by experience with dynamic-mode AFM interactions (Labardi, 1998), suggests that the double-modulation technique provides enhancement of the tip sharpening effect. In Section 3 we carry out a simple modelling, and establish some criteria for the interpretation of optical demodulated images at first and higher harmonics. Finally, in Section 4 a set of images taken on a test sample (described in Section 2) is shown, and the relevant features are discussed with special regard to artefact suppression, influence of sample geometry on near-field signal, effectiveness of the double-modulation technique, and possible application to near-field basic investigations.

2. Experimental set-up

SIAM was invented by H. K. Wickramasinghe and his collaborators at IBM Watson Research Center, Yorktown Heights (Zenhausern *et al.*, 1994) with the introduction of a scattering-type near-field sensor (a silicon tip) instead of an optical aperture. A similar idea was also introduced by Inouye & Kawata (1994) with a metallic tip. To overcome the sensitivity limits of intensity detection of the optical field, interferometric detection, already applied in a heterodyne configuration by Vaez-Iravani & Toledo-Crow (1993) to enhance contrast of aperture-type SNOM, was introduced in the homodyne configuration. The SIAM concept attained unprecedented optical resolution of less than 1 nm (Zenhausern *et al.*, 1995; Martin *et al.*, 1996), although accompanied by some debate of basic nature (Garcia & Nieto-Vesperinas, 1995) as well as concerning the possible presence of the *z*-motion artefacts pointed out by Hecht *et al.* (1997). The assessment of SIAM resolving power has stimulated researchers to improve experimental set-ups and to look for original solutions aimed to the suppression of background as well as of *z*-motion artefacts. As regards the optical resolution, it has been demonstrated to overcome 15 nm (Hamann *et al.*, 1998; Bridger & McGill, 1999). Such a limit is probably set by the available tip radius and detailed shape. As regards artefact suppression, operation in the constant height mode (CHM), or equivalently in the constant intensity mode (CIM), is a well assessed method for obtaining purely optical information, although not

employed practically owing to major technical difficulties in the imaging of samples that are not smooth on the nanometre scale on extended areas. Operation in the more practical constant gapwidth mode (CGM) has been demonstrated free of artefacts with the exploitation of higher harmonics demodulation (Labardi *et al.*, 2000a; Hillenbrand & Keilmann, 2000). Contrast enhancement is provided by the same method (Knoll & Keilmann, 2000; Labardi *et al.*, 2000a), that is indeed promising for overcoming the 10 nm resolution limit, at least on high optical contrast samples.

Our SIAM is structured as follows (Fig. 2). The beam of a laser diode ($\lambda = 780$ nm, $P_{out} = 25$ mW) is spatially filtered by a beam expander and crosses a polarizing beam splitter cube (PBSC) that acts as a good quality linear polariser in the 'vertical' direction, deviating away the 'horizontal' polarization part of the beam. After reflection by a mirror orientated at 45°, the beam crosses a Nomarski prism with optical axis orientated at 45° with respect to the polarization direction. This creates two slightly divergent, cross-linearly polarized beams with adjustable relative phase $\Delta\phi$. The beams are focused on the outer surface of the (transparent) sample by a 60× 0.85 numerical aperture (NA) microscope objective. The reflected spots, assumed to maintain the polarization, are collected by the same objective and cross back the Nomarski filter, that has no effect but to deviate the beams back to the original direction. After back-reflection by the 45° mirror, the beams cross back the PBSC. Its effect is now to let the vertical polarization component of each beam cross the cube, and deviate towards the detector their horizontal component. The detector is represented by a photodiode placed after a focusing lens and an interference filter at 780 nm used to cut off background ambient light. At the detector optical interference is realized, whose visibility is measurable by adjusting the relative phase of the two beams (Fig. 2) and results about 90% in our set-up, probably owing to the quality of the reflection at the sample.

The scattering probe is an AFM tip made of n^+-doped silicon, produced by Nanosensors™ (Nanosensors GmbH, Wetzlar-Blankenfield, Germany). The typical curvature radius of the tip is between 5 and 10 nm, and the aspect ratio better than 5 : 1. The tip is approached within the sample area illuminated by one of the beams and there maintained in the near-field region by tapping-mode AFM technique. The tip position can be controlled in x, y and z directions (standalone AFM configuration) while the sample is held at rest. Both tip and sample are mounted on piezoscanner tubes, but the one with the sample holder is kept at rest and moved only occasionally for test purposes.

Before proceeding to the working principles of the SIAM optical detection, it should be mentioned, for a better understanding, that the actual geometry of our system is built up in three dimensions, with the optical section (source, PBSC, detector) on the x-y plane and the SNOM section (mirror, Nomarski filter, objective, standalone AFM head) on the z axis, and that the sketch of Fig. 2 is a two-dimensional representation.

The optical detection operates as follows. Part of the light scattered by the tip in local interaction with the sample is collected by the high numerical aperture objective and enters the interferometer. The polarization of such light is unknown and its phase is related to the illumination beam where the tip is located. Variations of the interference signal due to the tip scanning are recorded and generically referred to as the optical image. Thus, the magnitude of the scattered field E_s is amplified by the homodyne factor $|E_r|/|E_s|$ where E_r is the total reflected field resulting from the interference of the couple of beams created by the Nomarski filter. Such amplification is responsible of the increased sensitivity of interferometric detection. Similar considerations are valid for optical heterodyne detection such as performed by Hillenbrand & Keilmann (2000).

The efforts made on our SIAM set-up for improving the overall performance and ease of operation are the following. To improve the standalone AFM system, an electromechanical proximity sensor similar to the one described by Rensen *et al.* (1999) has been developed, comprised of a quartz tuning fork, on which a cantilever is glued to form the AFM sensor, and of a miniaturized preamplifier mounted in the vicinity of the sensor itself. The system is operated in the tapping-mode at the tuning fork resonance frequency (about 32 kHz and depending on the cantilever attachment) for distance stabilization with calibrated oscillation amplitudes up to 100 nm peak-to-peak. Stable operation is obtained with the employment of the amplitude output channel of a dual-phase lock-in amplifier, and an integral feedback amplifier for the topography adjustment. The tuning fork is mechanically excited at resonance by a dithering piezoslab driven by a function generator. The actual fork oscillation is monitored, for calibration purposes, by means of an additional visible laser diode (not shown in Fig. 2) striking on one arm of the fork, and the diffraction pattern is detected by a small photodiode. This method is customarily used in aperture SNOM, and can be employed for absolute calibration of the probe motion (Wei *et al.*, 1995).

For the optical detection, an additional modulation is given to the fork far below resonance (1 kHz) through the dithering piezoslab. The optical signal is demodulated at such frequency by additional lock-in amplifiers (for simultaneous measurement of different harmonics). The double-modulation technique described here presents a number of advantages with respect to the case of single modulation: (1) optical signal is unaffected by mechanical contact effects on the cantilever motion that may change both the phase and amplitude of the instantaneous vibration and consequently the magnitude of the optical signal itself; (2) the

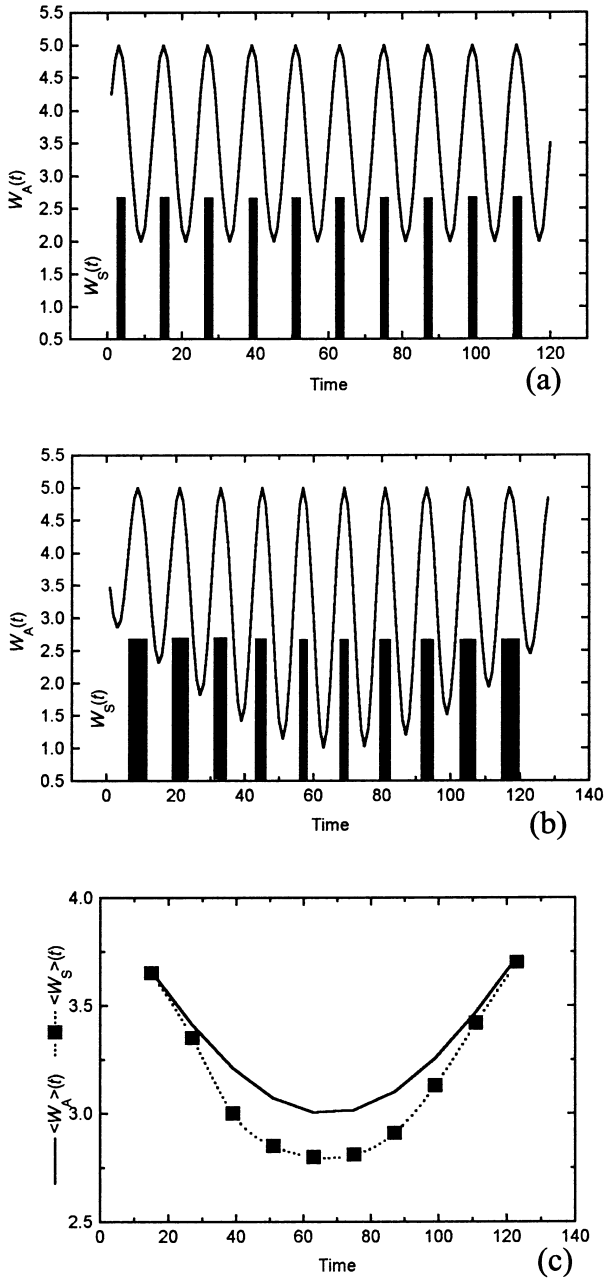

Fig. 3. Model for the optical response in the case of high modulation amplitude. (a) Time response owing to a simplified (step-like) form of the optical near-field, and to a possible artefact signal function (cosine) with single modulation; (b) same response in the case of double modulation for the near field and the artefact cases; (c) time integrals of the signals in (b).

lock-in amplifiers measuring the optical signal can be directly referenced to the excitation signal, as the off-resonance drive of the tuning fork ensures that the phase of the actual oscillation will correspond to the one of the excitation signal; and (3) amplitude of low frequency modulation can be changed at wish, in case of need, on a wide range (from 0 to the tapping-mode oscillation amplitude), with no consequences on distance stabilization.

The sample imaged is a close-packed latex sphere layer, deposited on glass. The diameter of the spheres is 500 nm. All the measurements have been performed in air and at room temperature, with a dielectric (silicon) tip.

3. Model

*n*th harmonic lock-in detection of the optical field scattered by the sinusoidally oscillating probe yields, for small displacement compared to the wavelength, a measurement of the *n*th spatial derivative of the field itself. The smaller the oscillation amplitude, the more rigorous the statement. In the tapping-mode, amplitudes can be rather high, up to 200 nm; in such a case, contributions of higher derivatives are present in the measurement (Labardi *et al.*, 2000b).

What happens in practice in the measurement process is as follows. Those optical fields that exhibit strong spatial variation on a scale comparable to the dithering amplitude of the probe will be enhanced after demodulation. For instance, an evanescent field with decay length d will be detected more efficiently when the probe is oscillated of a similar amplitude, because, in the first harmonic demodulation case, the probe experiences the stronger optical gradient during the oscillation cycle. This action can be regarded as a bandpass filtering of the spatial frequencies around $f_{xy} = 2\pi/d$ (Knoll & Keilmann, 2000; J. N. Walford, personal communication, 2000).

The double-modulation technique, where the optical field is measured at one frequency, and the tapping-mode distance control is performed at a much higher frequency, yields an effective increase of the bandpass centre frequency. This can be understood on a qualitative basis with reference to Fig. 3. Let us model the surface near field with a step function, that is, the signal due to the near-field scattering W_S will be some nonzero value (2.6 in our plot) when the tip is closer than some characteristic distance d from the surface (Fig. 1), and 0 otherwise. This is obviously an oversimplified form of a nonlinear signal function on the scale of d, like an evanescent wave. For the sake of simplicity, let us assume that the tapping-mode vibration amplitude A is such that $d << A << \lambda$. The artefact term W_A can be sketched in a realistic way by choosing a typical far-field spatial dependence, like a cosine function $\cos(4\pi z/L + \pi/4)$ (Labardi *et al.*, 2000a, b), that is characterized by a rather linear behaviour provided that $A << \lambda$.

Figure 3(a) shows the time diagram of the scattering signal W_S during several oscillation cycles of the probe at the tapping-mode modulation frequency f_1 (no additional modulation). The signal is composed by rectangular spikes, owing to the assumed step function. The width of one spike, that is the time τ spent by the probe in the near-field region,

is given by the equation:

$$(A - d)/A = \cos(2\pi f_1 \tau/2). \quad (1)$$

In the hypothesis $d << A$, its solution can be expanded to first order and gives:

$$\tau \approx (1/\pi)[2d/(f_1 A)]^{1/2}. \quad (2)$$

In a realistic case, the rectangular spike would be replaced by a more complicated shape, but the dependence on $A^{-1/2}$ would be roughly maintained, as it is due to the total time spent by the tip in the near-field region. As regards the time diagram of the artefact term W_A, shown in Fig. 3(a), it is given by a sinusoidal waveform, as far as linearity is assumed within the small oscillation region of the probe. It is worth noting that, within the present approximation, the surface near-field is seen as a whole, and its dependence on distance expressed by a single parameter d.

Let us now introduce the second modulation frequency $f_2 << f_1$ (Fig. 3(b)). As a result, the oscillation amplitude A becomes a function of time, spanning from $A - A_2$ to $A + A_2$ with period $T_2 = 1/f_2$. As a consequence, the width of the spike will be modulated, taking values in the range from $(A + A_2)^{-1/2}$ to $(A - A_2)^{-1/2}$. As regards the artefact term, it will be enveloped by a sine function as shown in Fig. 3(b). Note that the upper bound is given by the value of the optical field at contact. Let us now consider the result of a lock-in measurement on such signals at the frequency f_2. Roughly, the first harmonic will be proportional to the modulation depth of the function $<W_S>$ obtained by integration of W_S with a time constant $T = 1/f_1$ (Fig. 3(c), dots), that is still proportional to $d^{1/2}$ and, for $A_2 << A$, scales as $A \cdot A_2$. The same result for the artefact (Fig. 3(c), solid line) is a sinusoidal waveform, that is detected by first harmonic lock-in measurements and is proportional to the z-gradient of W_A.

The explanation of the 'sharpening' effect owing to the double modulation is thus the following. The most evident effect of the insertion of an additional modulation is the envelope of the oscillation span of the tip, from $A - A_2$ to $A + A_2$. When the oscillation amplitude amounts to $A - A_2$, the tip spends more time close to the surface. In the opposite case, the time spent near the surface is less. The interaction time depends on amplitude like $A^{-1/2}$; thus, the effect of amplitude reduction is more important in comparison to that of amplitude increase. This leads to an effective amplitude reduction, with consequent artefact reduction and increased sensitivity to near fields, and is at least in general agreement with more rigorous theoretical findings, based on the exploitation of reciprocity principle, presently under development (J. N. Walford, personal communication, 2000).

Higher harmonic detection provides no signal related to the artefact term, as far as W_A is assumed to be linear, that is, when the oscillation amplitude is small compared to the wavelength. On the contrary, the scattering term W_S contributes to the higher harmonics to a greater extent, as sketched in Fig. 3(c) where the term $<W_S>$ deviates from the sinusoidal form of $<W_A>$. For the case considered, nonlinearity derives from the dependence on the square root of d/A. However, in the case of A as small as to be comparable to d, the surface optical field cannot be represented by a step function anymore. In the more realistic case the field structure, that is, the detailed dependence of field amplitude on distance, becomes of importance. Namely, nonlinearities arise in the scattering term, while the artefact terms (first and higher harmonics) get smaller in proportion to the reduced oscillation amplitude A. Then it is plausible to attempt the reconstruction of the detailed near-field structure by measuring their higher order derivatives.

In a general case, nth harmonic lock-in measurements yield a response proportional to the nth spatial derivative, plus additional terms comprising higher order derivatives, as shown for the first and second harmonics by Labardi *et al.* (2000b), who explicitly calculated that the smaller the oscillation amplitude, the more faithfully lock-in detection accounts for the pure first- and second-order derivatives. Thus, the near-field structure could be analysed by addition of harmonics (moments) provided that the oscillation amplitude used for the measurements is small enough to ensure the validity of the 'derivative' approximation made.

The main conclusions that can be drawn, as regards the interpretation of apertureless optical imaging obtained by modulation techniques, are the following. By using high oscillation amplitude of the probe z-position, the near field interacts with the tip for short periods. In this case, our simple model shows that, given some interaction range d over the sample surface, the optical response $W_S(t)$ is such that its average value $<W_S>$ scales as $d^{1/2}$. Thus, the sensitivity to short-range interactions is enhanced by the modulation. Furthermore, for fixed d, reduction of the amplitude A yields more complicated shapes of the optical response that cannot be approximated like for the high amplitude case, and must be calculated explicitly. In the passive probe approximation, that is, by considering plausible forms for the surface fields not perturbed by the probe, calculations have been carried out by assuming exponential dependence (Adam *et al.*, 2000; Labardi *et al.*, 2000b). The passive probe approximation is justified when using dielectric tips, whereas in the case of metallic tips, interaction with the sample cannot generally be neglected. In this case, an image dipole model has been shown to yield an inverse power law used for calculating the optical response (Knoll & Keilmann, 2000). In the case of even smaller oscillation amplitudes, achievable, for instance, by operating in the non-contact mode of AFM, the response is the ideal one as regards the proper measurement of spatial derivatives, but on the other hand the signal level drops

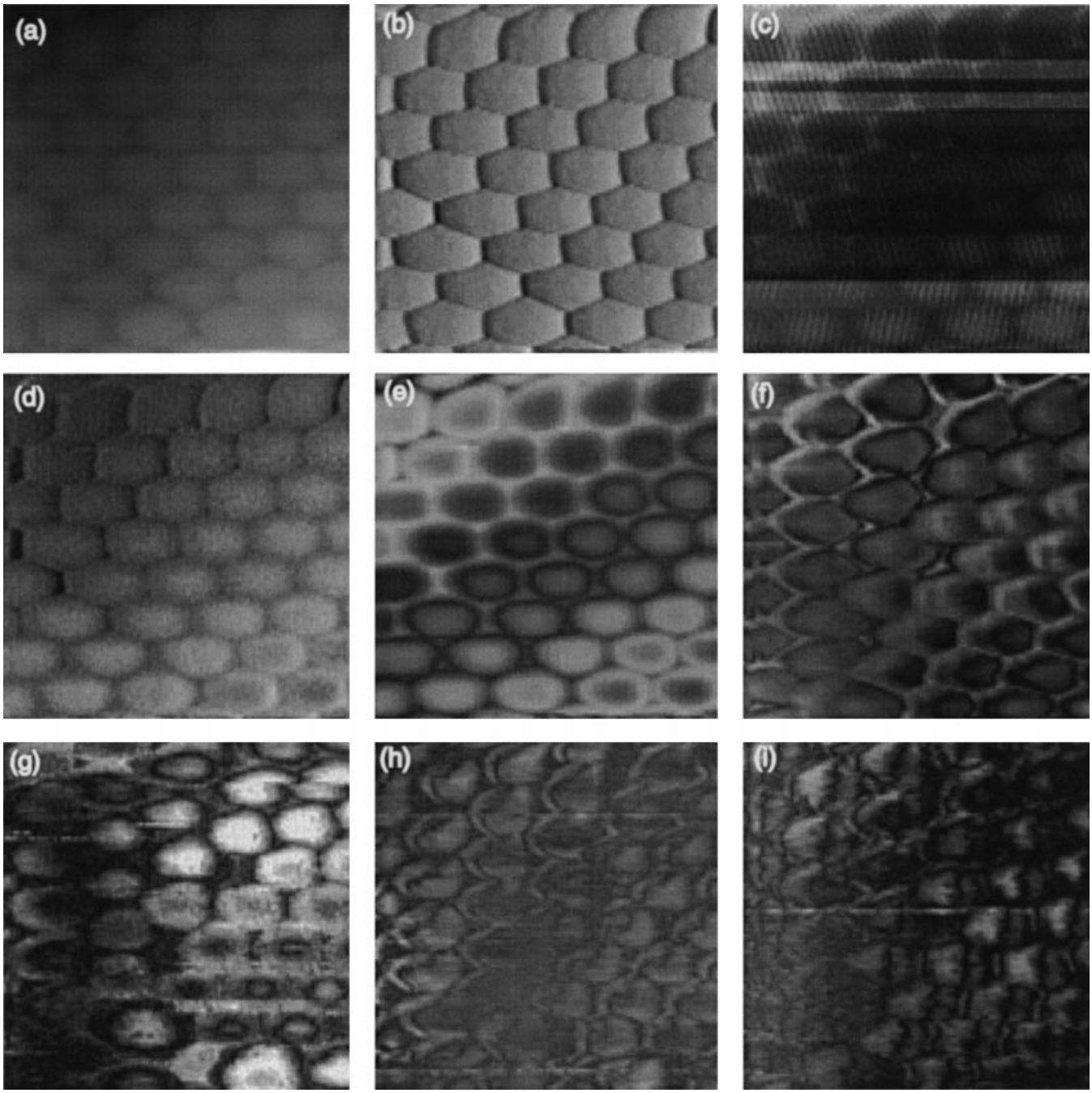

Fig. 4. Images of the test sample (close-packed latex spheres) recorded by scanning interference apertureless microscopy. (a) Topography (scan size 2.5 × 2.5 μm^2); (b) error signal; (c) d.c. optical signal; (d) first harmonic demodulated optical signal at the tapping-mode frequency (32 kHz); (e) first harmonic demodulated at the additional frequency (1 kHz); (f) second harmonic; (g) third harmonic; (h) fourth harmonic and (i) fifth harmonic. Tapping mode amplitude is 30 nm peak-to-peak; additional low frequency modulation is 6 nm peak-to-peak; sample rate is in the range 15–30 points s^{-1}, 128 × 128 points per image; images (a)–(e) are taken simultaneously; the images (g) and (h) and (f) and (i) are acquired in different scans. A small shift is visible between the images not taken during the same scan, although the relative position is easily recognizable and the corresponding topography and error signal are essentially unchanged and are not shown.

very likely to unacceptable values below the measurement noise limit, especially for the higher harmonic orders.

The insertion of an additional modulation frequency f_2 provides, in the case of high oscillation amplitude, an effect comparable to the reduction of the amplitude itself. In the case of smaller amplitude, such effect could be more pronounced, but in general the role of double-modulation to the image formation seems not to be crucial. The

usefulness of double-modulation is certainly more related to topographical artefact suppression and general convenience, for the reasons mentioned in Section 2.

In the following, the conclusions made will be applied to first SIAM measurements performed up to the fifth harmonic.

4. Results and discussion

The SIAM images (shown in Fig. 4) of the latex sphere sample are obtained with 30 nm peak-to-peak tapping-mode vibration, enveloped by a 6-nm peak-to-peak oscillation at 1 kHz. The setpoint of tapping-mode amplitude was indeed set at 60% of the free oscillation amplitude of 50 nm. The topographic adjustment was fairly stable for the whole measurement session reported here and no evident tip degradation has occurred whatsoever. Such stability has been assessed throughout a series of more than 10 scans (128×128 points), performed forward and backward at a rate variable from 15 to 30 points s^{-1}. The used operation mode was CGM with the topographic profiles showing spherical shapes with cusps in between.

In Fig. 4(a) the topographic image taken in CGM shows the structure of the sample used for our measurements. The scan size is $2.5 \times 2.5\ \mu m^2$, and the sampling distance (pixel to pixel) is about 20 nm. The top to cusp height measured on the spheres is about 230 nm, while the inclination plane contributes to about 500 nm, that is $0.65\ \lambda$. The local inclination angle of the sample is estimated around 8°. The dynamics of the error image (Fig. 4(b)) witnesses on the goodness of topographic tracking obtained. The feedback loop is mainly concerned in the compensation of the inclination plane while the response is flat while tracking the surface of one sphere, and a jump is recorded at the cusp between two spheres. Such jump, one pixel wide, is reflected in all optical images as well as in the error image. The d.c. optical signal (Fig. 4(c)) shows extremely reduced dynamics, about 2.4% change on the average value, comparable to the very small fluctuations of the laser diode power during the scan (lasting about 20 min), that amount to about 2%. The image shows a contrast inversion, happening along the diagonal of the frame, within a distance of (roughly) 2.5 μm. Such a direction complies with the orientation of the couple of spots created by the Nomarski filter. However, in this case we are in presence of a rather strong inclination of the sample in the same direction (along the diagonal), so that the observed variation could be assigned to a topographic artefact as well. It is already clear from this first optical image how z-motion artefacts may affect the SNOM optical maps: by adjusting its height, the tip introduces a phase shift $4\pi z/L$ on E_s. With a variation of $0.65\ \lambda$, such phase shift results 2.6π, that means, more than one full contrast inversion cycle should be visible within one scan, somehow more than observed. Then, the effect is probably due to the combination of z-motion artefact and illumination inhomogeneity over the scan area. The latter is also responsible for contrast inhomogeneities in the optical images at higher harmonics that will be shown briefly later on.

As already mentioned, the use the probe height modulation technique, preferably at harmonics higher than the first, represents a very effective way to suppress z-motion artefacts, as well as to reject slowly varying far-field components. For comparison, we have acquired the first harmonic demodulated optical signal, both at the tapping-mode frequency (as often done in other set-ups) and at the additional modulation frequency. The comparison is shown in Figs 4(d) and (e), respectively. It is clearly seen that the first harmonic optical image at 32 kHz resembles the error image (b). A strict link is expected between them, as faulty amplitude feedback control will exactly show up in the optical image demodulated at the tapping-mode frequency. Image (e), recorded at 1 kHz, resembles more the dc optical image (c), with much higher signal-to-noise ratio. Also the topography-induced artefact seems to be enhanced here; indeed, the contrast inversion is strikingly evident even within a single sphere.

The modulation used for Figs 4(d) and (e) is quite different. In Fig. 4(d) we use the single modulation technique, with 30 nm peak-to-peak amplitude. In Fig. 4(e) we use the double modulation with an additional 6 nm peak-to-peak amplitude envelope at 1 kHz. Note that all of the images discussed up to now have been acquired simultaneously, that is, it is meaningful to analyse pixel-to-pixel correspondence between them. The result confirms that the single modulation image Fig. 4(d) is dominated by the perturbations of the topography tracking system that mix to the optical signal, while the latter effect is much reduced with the double modulation technique, where the presence of the z-motion artefact is still important.

Let us now examine the higher harmonics images, Figs 4(f)–(i) for harmonics from second to fifth, respectively. These images have been taken neither simultaneously to the previous ones nor among them, with the exception of the Figs 4(f) and (i). Nevertheless, a number of observations can be done. One, the borders of the spheres are enhanced. This is sound on a general basis, and in agreement with the conclusions of our model, that anticipates enhanced sensitivity to near fields that can be described by characteristic distances somehow smaller than $A = 30$ nm, due to the double-modulation technique, and that should be present at the borders of structures also in the case of homogeneous optical constants (Adam *et al.*, 2000). Second, asymmetry of the optical appearance of the spheres comes out, with marked differences between the various harmonics. Such appearance is fairly coherent within one frame, that is, does not depend too much on the position of the sphere in the frame, especially in Figs 4(h)

and (i). The optical appearance at the different harmonics could be used to build up the detailed near-field distribution of one sphere of the close-packed layer, by means of addition of harmonics. The use of a silicon tip ensures the validity of the passive probe approximation, where the surface fields are assumed not to be perturbed by the presence of the probe. Thus, the developed imaging technique could be used for multipolar near-field reconstruction, and thus provide clear experimental evidence of geometrical near-field effects on nanometre-size structures. At present, however, this task requires further technical study before being applicable to practical cases.

No relevant contrast inversion effects are visible within the scan area, especially for the higher harmonics, and the interstices among the spheres do not generally invert their contrast with respect to the spheres themselves, contrarily to what observed in d.c. (Fig. 4(c)) and first harmonic (Fig. 4(e)) optical images. This is a clear indication of the achieved artefact-free imaging character, that is improved by the harmonic order. Variation of contrast within the image can be attributed to the inhomogeneity of the illumination.

Finally, the relative weight of the higher harmonics, calculated from the maximum value of the optical signal on each image, and normalized to 100% for the first harmonic, is roughly: 20% (second), 2.9% (third), 1.1% (fourth), 1.1% (fifth). These values might be compared with theoretical estimations, provided that the effect of the double modulation is taken into account in the calculations. However, it is evident from these figures that the magnitude of higher harmonics have overcome a strong enhancement.

5. Conclusions

Visualization of higher harmonics (up to the fifth) of the modulated optical signal owing to vertical probe oscillation has been accomplished by a scanning interference apertureless microscope, where the tip z-position is modulated with two frequencies simultaneously. The higher frequency (32 kHz, 30 nm peak-to-peak) provides the tapping-mode AFM distance stabilization, while the lower one (1 kHz, 6 nm peak-to-peak) is the one where the optical signal is detected by nth harmonic lock-in technique with $n = 0–5$. The present work demonstrates that higher moments of the surface optical field can be mapped by using a dielectric tip, in order to comply with the passive probe approximation, and can provide either artefact-free optical imaging, or the detailed structure of the near-field scattered by the surface.

Acknowledgements

We are very grateful to Vahid Sandoghdar and Thomas Kalkbrenner, University of Konstanz, for providing the test sample, and to J. N. Walford, Ecole Centrale, Paris, for stimulating discussions. We thank for financial support INFM-MURST through the project 'SUD-NanoSNOM', and EC within the TMR Network 'Near Field Optics for Nanotechnology.'

References

Adam, P.M., Bijeon, J.L., Viardot, G. & Royer, P. (2000) Analysis of the influence of the tip vibration in the formation of images in apertureless scanning near-field optical microscopy. *Opt. Commun.* **174**, 91–98.

Bachelot, R., Gleyzes, P. & Boccara, A.C. (1997) Reflection-mode scanning near-field optical microscopy using an apertureless metallic tip. *Appl. Opt.* **36**, 2160–2170.

Bridger, P.M. & McGill, T.C. (1999) Observation of nanometer-scale optical property discrimination by use of a near-field scanning apertureless microscope. *Opt. Lett.* **24**, 1005–1007.

Brunner, R., Simon, A., Stifter, T. & Marti, O. (2000) Modulated shear-force distance control in near-field scanning optical microscopy. *Rev. Sci. Instrum.* **71**, 1466–1471.

Garcia, N. & Nieto-Vesperinas, M. (1995) Theory for the apertureless near field optical microscope image-resolution. *Appl. Phys. Lett.* **66**, 3399–3400.

Hamann, H.F., Gallagher, A. & Nesbitt, D.J. (1998) Enhanced sensitivity near-field scanning optical microscopy at high spatial resolution. *Appl. Phys. Lett.* **73**, 1469–1471.

Hecht, B., Bielefeldt, H., Inouye, Y., Pohl, D.W. & Novotny, L. (1997) Facts and artifacts in near-field optical microscopy. *J. Appl. Phys.* **81**, 2492–2498.

Hillenbrand, R. & Keilmann, F. (2000) Complex optical contrast on a sub-wavelength scale, *Phys. Rev. Lett.* **85**, 3029–3032.

Inouye, Y. & Kawata, S. (1994) Near-field scanning optical microscope with a metallic probe tip. *Opt. Lett.* **19**, 159–161.

Knoll, B. & Keilmann, F. (2000) Enhanced dielectric contrast in scattering-type scanning near-field optical microscopy. *Opt. Commun.* **182**, 321–328.

Labardi, M. (1998) Apparent and actual damping in dynamic force spectroscopy. *Probe Microscopy*, **1**, 215–224.

Labardi, M., Patanè, S. & Allegrini, M. (2000a) Artifact-free near-field optical imaging in apertureless microscopy. *Appl. Phys. Lett.* **77**, 621–623.

Labardi, M., Patanè, S. & Allegrini, M. (2000b) Modulation techniques in near-field optical microscopy. *Proc. Int School Physics 'Enrico Fermi', Course CXLIV 'Nanometer Scale Science Technology', Società Italiana di Fisica, Bologna*, M. Allegroni, N. Garcia and O. Marti (Eds). 105 Press, Amsterdam.

Lieberman, K., Ben-Ami, N. & Lewis, A. (1996) A fully integrated near-field optical, far-field optical, and normal-force scanned probe microscope. *Rev. Sci. Instrum.* **67**, 3567–3572.

Martin, Y., Zenhausern, F. & Wickramasinghe, H.K. (1996) Scattering spectroscopy of molecules at nanometer resolution. *Appl. Phys. Lett.* **68**, 2475–2477.

Porto, J.A., Carminati, R. & Greffet, J.J. (2000) A theory of near-field optical imaging. *J. Appl. Phys.* **88**, 4845–4850.

Rensen, W.H.J., Van Hulst, N.F., Ruiter, A.G.T. & West, P.E. (1999) Atomic steps with tuning-fork-based noncontact atomic-force microscopy. *Appl. Phys. Lett.* **75**, 1640–1642.

Vaez-Iravani, M. & Toledo-Crow, R. (1993) Phase-contrast and amplitude pseudoheterodyne interference near-field scanning optical microscopy. *Appl. Phys. Lett*. **62**, 1044–1046.

Wei, C.-C., Wei, P.-K. & Fann, W. (1995) Direct measurements of the true vibrational amplitudes in shear force microscopy. *Appl. Phys. Lett*. **67**, 3835–3837.

Zenhausern, F., Martin, Y. & Wickramasinghe, H.K. (1995) Scanning interferometric apertureless microscopy: optical imaging at 10 Angstrom resolution. *Science*, **269**, 1083–1085.

Zenhausern, F., O'Boyle, M.P. & Wickramasinghe, H.K. (1994) Apertureless near-field optical microscope. *Appl. Phys. Lett*. **65**, 1623–1625.

Zhong, Q., Inniss, D., Kjoller, K. & Elings, V.B. (1993) Fractured polymer/silica fiber surface studied by tapping mode atomic force microscopy. *Surf. Sci. Lett*. **290**, L688–L692.